MICROLENSING PARALLAX FOR OBSERVERS IN HELIOCENTRIC MOTION

S. CALCHI NOVATI[1,2,3,4] AND G. SCARPETTA[2,3]

[1] NASA Exoplanet Science Institute, MS 100-22, California Institute of Technology, Pasadena, CA 91125, USA
[2] Dipartimento di Fisica "E. R. Caianiello," Università di Salerno, Via Giovanni Paolo II, I-84084 Fisciano (SA), Italy
[3] Istituto Internazionale per gli Alti Studi Scientifici (IIASS), Via G. Pellegrino 19, I-84019 Vietri Sul Mare (SA), Italy

ABSTRACT

Motivated by the ongoing *Spitzer* observational campaign, and the forthcoming *K2* one, we revisit, working in an heliocentric reference frame, the geometrical foundation for the analysis of the microlensing parallax, as measured with the simultaneous observation of the same microlensing event from two observers with relative distance of order au. For the case of observers at rest, we discuss the well-known fourfold microlensing parallax degeneracy and determine an equation for the degenerate directions of the lens trajectory. For the case of observers in motion, we write down an extension of the Gould relationship between the microlensing parallax and the observable quantities and, at the same time, highlight the functional dependence of these same quantities from the timescale of the underlying microlensing event. Furthermore, through a series of examples, we show the importance of taking into account the motion of the observers to correctly recover the parameters of the underlying microlensing event. In particular, we discuss the cases of the amplitude of the microlensing parallax and that of the difference of the timescales between the observed microlensing events, which are key to understand the breaking of the microlensing parallax degeneracy. Finally, we consider the case of the simultaneous observation of the same microlensing event from the ground and two satellites, a case relevant for the expected joint *K2* and *Spitzer* observational programs in 2016.

Key words: gravitational lensing: micro

1. INTRODUCTION

The microlensing parallax is a key observable to break the degeneracy in the microlensing parameter space and recover the physical parameters of the lens, specifically its mass and distance. The framework for the analysis of the microlensing parallax, through measures from two observers distant enough one from the other, and specifically through the simultaneous observation of the same microlensing event from ground and from space, has been set by Refsdal (1966) and later brought up to date and developed by Gould (1994). The era of space-based microlensing parallax observations began using *Spitzer* (Werner et al. 2004), as earlier suggested by Gould (1999), with the analysis of a SMC event (Dong et al. 2007), and continued with the ongoing *Spitzer* observational campaign, which was started in 2014 for the follow up of microlensing events detected toward the Galactic bulge led by A. Gould (Gould et al. 2013, 2014, 2015a, 2015b). This observational campaign has led to several important results, which clearly shows the importance of these kinds of measurements, among which include the first microlensing exoplanetary system with a space-based parallax measurement (Udalski et al. 2015), the first space-based microlens parallax measurement of an isolated star (Yee et al. 2015b), and the first analysis of one of the main goals of the campaign: the determination of the Galactic distribution of exoplanets (Calchi Novati et al. 2015a; for this specific issue we also refer to the recent analysis by Penny et al. 2016). Furthermore, in the next few years the space-based microlensing parallax is expected to play an increasingly relevant role for the analysis of microlensing events, in particular for the characterization of exoplanets, in addition to *Spitzer* also with *K2* (Howell et al. 2014) and, in the longer term, with WFIRST (Spergel et al. 2015; for specific analyses

on the microlensing parallax with WFIRST, we refer to Gould 2013; Yee 2013).

A key aspect in the analysis of space-based microlensing parallax events is to understand the underlying degeneracy for the parallax determination: a fourfold degeneracy of the direction of the parallax "vector" and a twofold degeneracy of the parallax amplitude, which is the relevant quantity to determine the physical characteristics of the lens system. As further detailed below, this degeneracy arises because the observation of the same microlensing event from two observers only partly breaks down the degeneracy among the directions of the lens-source relative motion, a degeneracy that is instead complete for the observation by a single observer of a single-lens microlensing event. Gould (1994) set the framework for analyzing the microlensing parallax in the case of two inertial observers at rest. Gould (1995) then addressed the issue of the parallax degeneracy for the case of two observers in relative motion, but still from within the framework established for the case of inertial observers at rest. The results of these works then became the basis for the analysis of the mechanism for breaking the parallax degeneracy, and in particular for two simulations of the microlensing parallax signal toward the Magellanic Clouds (Boutreux & Gould 1996) and the Galactic bulge (Gaudi & Gould 1997). Incidentally, we recall that these are two opposite observational targets because they lie, roughly, at the ecliptic pole and along the ecliptic plane, respectively; the second line of sight is coplanar with typical satellite orbits, and specifically for that of *Spitzer* and *Kepler*.

The recently renewed and growing observational importance of space-based microlens parallax calls for a better theoretical understanding of its underlying mechanisms, in particular for the breaking of the degeneracy for observers in relative motion. Addressing this issue is the primary goal of the present work. Specifically, we extend the Gould (1994) expression relating

---

the microlens parallax to the light curve observable at rest to the general case of observers in motion. Considering the line of sight toward the Galactic bulge, which is currently the most relevant from an observational point of view, we then present a series of microlensing event test cases to show the impact of including the motion of the observers in the analysis, by comparing our results with the outcome of the Gould (1995) analysis. We perform our analysis from the ideal point of view of an observer—within an heliocentric frame—which can be considered inertial to excellent approximation. Contrary to the usual choice of a geocentric point view, allows a clearer and more transparent discussion of the problem.

The microlens parallax is a genuine geometrical effect. The strength of its measure with simultaneous ground- and space-based observations is enhanced by its clean signature on the light curves, which usually results in rather precise determinations (e.g., the typical relative error for the parallax in single-lens systems in Calchi Novati et al. 2015a is about 10%). Besides the error on the single parallax solutions, however, a major source of uncertainty remains associated with the discrete degeneracy in the microlensing parallax determination. This framework, to the extent that it may break down this degeneracy, is where a combined space-based analyses, as the expected joint observations with *Spitzer* and *K2*, may be of key importance. Considering the determination of the physical lens parameters, in particular the lens mass, we recall however that aside from the event duration, the measure of the microlensing parallax alone is not sufficient to break down the degeneracy in the microlensing parameter space. The overall error budget for the physical parameters is therefore the result of the combined effects of all measurable quantities. The degeneracy may be broken if, besides the microlensing parallax, one can evaluate the Einstein angular radius through the observation of the finite source effect. This is routinely measured in multiple-lens planetary systems, but only infrequently in single-lens ones. Out of the 2015 *Spitzer* campaign (Calchi Novati et al. 2015b), Zhu et al. (2015) reported two such (single-lens system) cases, achieving a relative error for the lens mass of 15% and 8%. The two planetary systems with *Spitzer*-based microlens parallax, OGLE-2014-BLG-0124 (Udalski et al. 2015) and OGLE-2015-BLG-0966 (Street et al. 2016), come with a relative error in the planet mass determination of 30% and 10%, respectively, where, in the first case, the error budget is dominated by the uncertainty related to the finite source effect. A different channel for breaking the degeneracy in the lensing parameter space, independent bfrom the measure of the microlens parallax and suitable for ground-based observations only, is based on the measure of the lens flux and the relative lens-source proper motion (the second is key to unambiguously disentangle the lens and the source flux; Henderson et al. 2014). This kind of analysis must wait a few years after the peak magnification and requires high angular resolution imaging facilities, ground-based adaptive optic systems, or space observatories (e.g. the *Hubble Space Telescope*). In this framework Bennett et al. (2015) and Batista et al. (2015) recently reported on their analyses of the planetary system OGLE-2005-BLG-169 (Gould et al. 2006), where they reach a precision of 6% in the planet mass determination.

The paper is organized as follows. In Section 2 we set the framework of our analysis: in Section 2.1 we describe the case of the microlensing parallax for two observers at rest within an heliocentric frame, and in particular we go through a detailed geometrical analysis of the underlying degeneracies; in Section 2.2 we extend the analysis to the case of observers in motion. In Section 3 we present an analysis of the parallax for sample light curves for the line of sight toward the Galactic Bulge. In Section 4 we discuss the case for the simultaneous observation of the same microlensing event from the ground and two satellites, which is what we expect to happen during the *K2* and *Spitzer* microlensing campaign in 2016.

2. THE MICROLENSING PARALLAX

We start by setting the framework and the notation of our analysis. Through the paper we consider a single-point source single-lens system. A microlensing event (for a review see, e.g., Mao 2012) is then characterized by three parameters: the time at maximum magnification, t_0; the impact parameter, u_0, which sets the magnification at maximum along the microlensing light curve at $t = t_0$; and the *Einstein time*, t_E, which sets the timescale of the event. The light curve magnification, which is the typical bell-like symmetric shape known as Paczyński light curve (Paczyński 1986), reads

$$A(t) = A(u(t)) = \frac{u^2 + 2}{u\sqrt{u^2 + 4}}, \quad u(t) = \sqrt{u_0^2 + \left(\frac{t - t_0}{t_E}\right)^2},$$
(1)

where $u(t)$ describes the relative distance, projected on the lens plane orthogonal to the line of sight to the source, of the lens with respect to the observer.

The expression for $u(t)$ in Equation (1) holds for linear uniform lens motion with respect to an inertial observer; it is an excellent approximation for typical microlensing events, lasting from days up to few months, for an ideal observer on the Sun. Furthermore, Equation (1) also works well for observers on Earth, except for very long timescale events where the orbital motion comes into play.

All the physical parameters of the source-lens system are enclosed in the event timescale, the *Einstein time* $t_E = R_E/v$, where v is the relative lens-source velocity on the lens plane. The *Einstein radius*, R_E, is the characteristic length of the system, with all the physical lengths on the lens plane being normalized with it. The Einstein radius is a function of the distance from the observer to the lens, D_l, the source, D_s, and of the lens mass, M_l. The *microlensing parallax*, π_E, is defined as the inverse of the Einstein radius, in units of au, projected on the observer plane, $\pi_E = \mathrm{au}(1 - x)/R_E$, where $x \equiv D_l/D_s$. We recall that for Galactic bulge events R_E is typically of order au. (This is the underlying reason why the two observers must lie at about a relative distance of order au to measure the microlensing parallax. The exceptions are the rare cases of the extremely highly magnified microlensing events for which the microlensing parallax can be determined from two observers separated by about 1 Earth radius; Gould 1997). We recall that the choice of the microlensing parameters is not univocal, in particular, the formalism can be more suitably (for several applications) recast in terms of observables (Gould 2000).

In principle, one may further characterize a microlensing event by giving the direction of the lens relative motion in the lens plane, although this remains completely undetermined in Equation (1) because it only contains the modulus of the impact parameter. However, the direction of motion is relevant when discussing the parallax, so that we introduce, as a fourth parameter, the angle χ between a fixed direction (in our

notation, the x-axis of the reference frame will be introduced in Section 2.1) and the orthogonal to the direction of the lens motion.

The three parameters, t_0, u_0, and χ, all characterize the geometry of the microlensing event. The first two do not carry any information on the physical parameters of the lens system, as their underlying distribution is indeed flat. The case of χ is different, though, as its distribution reflects that of the underlying lens and source velocity, and therefore is endowed with an intrinsic, often relevant, physical information.[5]

Note finally that in the following we always refer to the microlensing parameters t_0, u_0 and t_E, without further subscript, as those of the underlying microlensing event that would be seen from the ideal observer on the Sun.

2.1. Observers at Rest in an Heliocentric Reference System

In this section we revisit the analysis of the microlensing parallax with observers at rest within a heliocentric framework. This approach provides us with a different point of view on well-known results and, at the same time, leads us to highlight some relationships that, to our knowledge, may not have been discussed already. Furthermore, this gives us the necessary basis to discuss the case with observers in motion.

We consider a heliocentric cartesian frame on the lens plane, centered along the line of sight to the source, as seen from the Sun. The choice of the reference frame within the lens plane is then arbitrary modulus a rotation in this plane. The orbital motions of the observers all take place on the ecliptic plane, which takes a privileged position. The "canonical" choice for the reference frame in the lens plane, from a geometrical point of view, would then be that of having one of the axes pointing along the line of nodes, which is the intersection of the ecliptic plane with the lens plane. Following the established habit in literature, however, we fix the x-axis along the line of the nodes intersection of the lens plane with the equatorial plane instead, in particular with the x and y axes pointing along the equatorial coordinates, west and north, respectively. We note however that because the line of sight we consider is pointing toward the Bulge, roughly on the ecliptic plane, and at $\lambda \sim 270°$, these two choices almost coincide.

We consider an observer at rest out of the origin, which can be the Earth approximated at rest. Its position in the lens plane, as given by the intersection of its line of sight to the source with the lens plane, then depends, aside from its position in the observer plane, only on the microlensing parallax. Specifically, its distance from the origin scales with the microlensing parallax.[6] Because of this offset from the origin, the observer would see the same microlensing event as the (ideal) observer in the origin, with the same timescale t_E, but a different impact parameter and time at maximum magnification. Now we introduce a second observer lying into the same observer plane, which we are going to identify with the satellite *Spitzer*, and which for now we also consider to be at rest. The relative distance between the two observers, a known quantity in the

observer plane, when projected in the lens plane also scales with the microlensing parallax (Gould 1994)

$$\vec{\pi}_E = \vec{\pi}_{E,\pm,\pm} = \frac{au}{D_\perp}(\tau, \Delta u_{0,\pm,\pm}),$$

$$\tau = \frac{t_{0,2} - t_{0,1}}{t_E}, \quad \Delta u_{0,\pm,\pm} = \pm(|u_{0,2}| \pm |u_{0,1}|). \quad (2)$$

Here $t_{0,1}$, $t_{0,2}$ and $u_{0,1}$, $u_{0,2}$ indicate the time at maximum magnification and the impact parameter of the microlensing event as seen by the two observers, and $D_\perp$ is the relative physical distance between the two observers in the lens plane, expressed in au. For reference, in the following we will always identify the observer "1" as that on Earth. This expression is key for the measurement of the microlensing parallax that is expressed in terms of all observable quantities.

The basis of Equation (2) lies on elementary geometrical considerations that can be done looking at Figure 1, as further discussed below. The notations $\pm$, $\pm$ in Equation (2) refer to the aforementioned fourfold degeneracy in the vector parallax determination, and twofold degeneracy in the modulus, $\pi_{E,\pm}$, which we now describe in some detail.

In Figure 1 we represent the four degenerate configurations for the geometry of a microlensing event projected on the lens plane, as seen by the two observers (Earth and *Spitzer*). We draw a circle of radius u_0 centered on the origin. From the point of view of the ideal observer in the origin (the Sun), the observed light curve is compatible with whatever lens motion direction is tangent to this circle. However, the angle χ singles out a unique lens direction, with the lens passing at the tangent point at time t_0. We can draw similar circles around the observer positions on the lens plane, with radius $u_{0,1}$ and $u_{0,2}$, respectively. Geometrically, the lens trajectory must then be tangent simultaneously to all the three circles, with $t_{0,1}$ and $t_{0,2}$ being the times of passage of the lens at the respective tangent points.

Following (and with some abuse of notation) Equation (2), we introduced the parallax "vector," $\vec{\pi}_E$, with components projected along and perpendicular to the lens motion. The amplitude of the parallax vector, the microlensing parallax π_E, is then obtained applying the Pythagoras theorem to the right angle triangle whose hypotenuse is given by the distance between the two observers, and whose cathetus are equal, respectively, to the distance between the tangent points of the two observer circles and to the difference of the observers' impact parameters (Figure 1, top panels).

An expression for $\tau = \Delta t_0 / t_E$ as a function of the parameters of the underlying microlensing event is

$$\tau = \pi_E(\cos(\chi)\Delta y_0 - \sin(\chi)\Delta x_0), \quad (3)$$

where $(\Delta x_0, \Delta y_0)$ are the distances of the observers' position projected on the lens plane, with $D_\perp$ in Equation (2) equal to $\sqrt{(\Delta x_0)^2 + (\Delta y_0)^2}$. In Equation (3) Δt_0, Δx_0, and Δy_0 are all intended to be signed quantities, as well as t_E, whose sign can identify the versus of motion along a given direction. Our sign convention is that, looking the lens plane as in Figure 1, the lens motion is anti-clockwise at the tangent point between the lens trajectory and the circle of radius u_0 centered in the origin. We also note that τ is invariant upon a change in the direction of motion (which corresponds to a simultaneous change in the sign of t_E and therefore also of Δt_0). Equation (3) follows from

---

[5] From an observational point of view the distribution for u_0 is not flat. This reflects both the efficiency of a given instrumental setup and therefore, indirectly, also the underlying source luminosity function.

[6] From an analytical point of view, this holds within the usual approximation of neglecting the lengths in the observer plane, of order au, compared with the distance to the source, of order kpc. We note that this is the same approximation within which we can mix up geocentric and heliocentric equatorial coordinates.
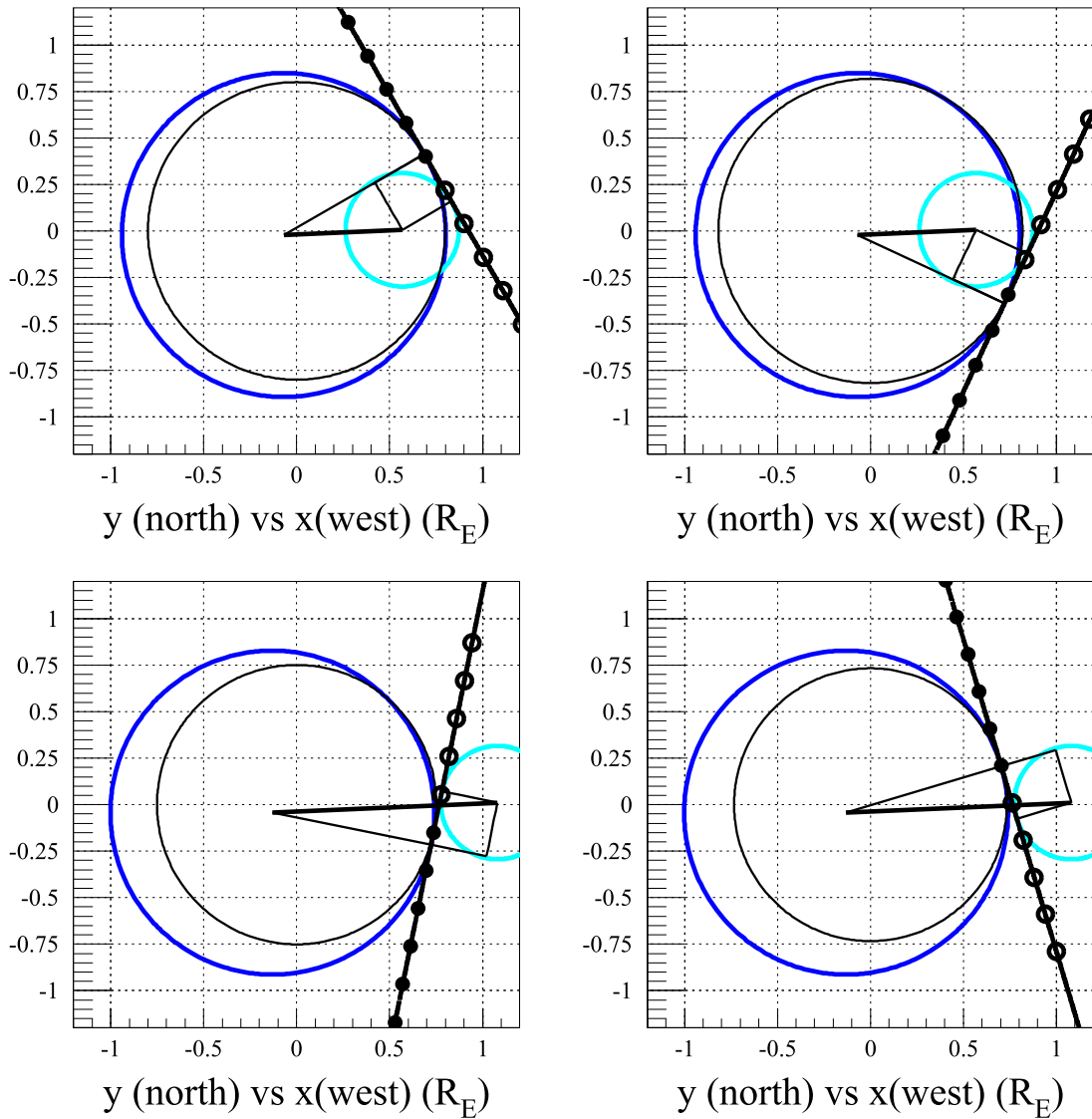
Figure 1. Projected in the lens plane, in a heliocentric reference frame centered on the line of sight to the source, the four degenerate configurations for the same microlensing light curves as observed by two observers at rest on Earth and *Spitzer* for a line of sight toward the Bulge (see Section 2.1 for full details). Top (bottom) panels for the $\pi_{E,-}$ ($\pi_{E,+}$) configurations, respectively. The thin black circle is centered on the origin, radius the impact parameter as would be seen from the Sun. The thick circles are centered on the observer positions, with radius the respective impact parameters, dark and light blue for Earth and *Spitzer*. The straight lines simultaneously tangent to the three circles represent the lens trajectory, the dots along it are equally spaced by five days, with empty ones for times prior t_0. The centers of the Earth and *Spitzer* circles are joined by a thick line, whose length scales with the microlensing parallax; the thinner lines indicate the triangle construction underlying Equation (2). The x and y axes are along the equatorial directions (west and north, respectively), and the z-axis along the line of sight, as seen from the Sun.

the geometry of the problem, and is therefore implicit in Equation (2) (in particular it is closely related to Equation (8) in Gould 2004), however to our knowledge it was not previously explicitly written down. In particular, it relates the projections of the components of $D_\perp$ along the lens trajectory to the distance between the two tangent points to the observer circles, which is equal to the difference of the observers' time at maximum magnification in units of the Einstein time (we recall that all the distances are normalized by R_E). This equation is important because, together with Equation (2), it provides the basic analytical understanding of the underlying fourfold degeneracy. Specifically, it shows that τ only depends, aside from the known observers' position, on π_E and χ. Namely, in addition to being independent from the event timescale, which is obvious because the parallax is intrinsically a static quantity,

τ is also independent from the impact parameter and the time at maximum magnification of the underlying microlensing event. This is key to explaining the parallax degeneracy. When τ and π_E are fixed, Equation (3) can become an equation for χ, and, in agreement with the geometry shown in Figure 1, it is a quadratic equation (see also Gould 2014 for a discussion of the widespread appearance of quadratic equations in microlens parallax). Namely, two possible lens trajectories are compatible with the light curves as seen from the two observers, corresponding to the two simultaneous tangents to the observers' circles. From a geometrical point of view, the degeneracy follows in that we cannot establish whether the observers lie both "above" or "below" the lens trajectory (Figure 1, top panels). Analytically, the key point is the freedom left by the independence of τ from u_0 and t_0 (and t_E).

Once χ is fixed according to Equation (3), we can independently fix u_0 so that the trajectory is tangent to the two observers' circles so as to this recover the observable values $u_{0,1}$ and $u_{0,2}$, and, furthermore, suitably shift t_0 to get the same observable times at maximum magnification (for a given value of the timescale). Finally, we note that following the habit, we consider the observer impact parameters as signed quantities, although, because they are intrinsically positive, geometrically they express a distance. The sign indicates whether the observer position at maximum magnification lies in the same semiplane set by the lens trajectory as the origin, or not (the sign being conventionally positive or negative, respectively), defining a kind of "parity" for the configuration.

The configuration for the two top panels in Figure 1, with the observers lying in the same semiplane with respect to the lens trajectory (which in principle can be the same or not as that of the observer in the origin) is said to be $\pi_E = \pi_{E,-}$, with the subscript—to indicate that in Equation (2) we take the difference of the impact parameters.

Given the same values for the observer impact parameters and τ, from Equation (2) we can then evaluate a second value for the parallax amplitude, $\pi_E = \pi_{E,+}$, taking the sum of the observers' impact parameters. This case corresponds to the geometry configurations shown in Figure 1, bottom panels, with the observers now lying on the opposite sides of the lens trajectory. The new directions for the lens trajectories can be determined by Equation (3), for which we can find suitable values of u_0 and t_0 to reproduce exactly the same observed light curves. This completes the fourfold parallax degeneracy for observers at rest. The geometry for the same couple of $u_{0,1}$ and $u_{0,2}$ is fixed by π_E (two possible values), χ and u_0 (for possible values each), regardless of the event timescale. Given the geometry, the event timescale fixes the observed difference of the times at maximum magnification.

As a technical point, we note that whereas Equation (3) can be used only to determine the directions of the lens trajectories, the full equations, namely including u_0, can be obtained from a geometrical analysis looking for the simultaneous tangents to the two observers' circles, with the constraint that the distance from the two tangent points must remain equal to τ. This way, through simple algebra, we can fully analytically recover the parameters of the four degenerate underlying microlensing events giving rise to the observed light curves.

In Figure 2, top panel, we show the light curves corresponding to the four degenerate configurations shown in Figure 1. In the middle and bottom panels, we fix the configuration to the four underlying degenerate microlensing events (and therefore for appropriate different values for u_0 and t_0) and let the angle χ vary. For each given configuration, we show the variation for Δt_0, middle panel (Equation (3)), and, bottom panels, for the observers' impact parameters, $u_{0,1}$ and $u_{0,2}$. In particular $u_{0,2}$ moves to negative values, whereas $u_{0,1}$ remains at the same time positive value, corresponding to the configuration with the two observers lying on opposite sides with respect to the lens trajectory (which is indeed always the case for the $\pi_{E,+}$ configurations). The dotted vertical lines indicate the values of the angle χ corresponding to the degenerate configurations. We note that for each configuration there are two values of χ for which we get the same value for Δt_0, but these come with different values of the impact parameters.

For reference, the numerical values that fix the configurations shown in Figures 1 and 2 are as follows. The line of sight toward the Bulge is fixed at R.A., decl. $= 266°.8, -21°.4$ (with ecliptic latitude $\beta = 2°.0$), with the source; hereafter we always assume the Bulge at $D_s = 8$ kpc. We arbitrarily fix the observer positions at the Earth and *Spitzer* positions along their orbits (as discussed in Section 2.2) at $t = $ (JD-2450000) $= 6836.0$ (2014 June 27). The four underlying degenerate microlensing event configurations for timescale $t_E = 24$ day have parameters (top to bottom, left to right in Figure 1)
$t_0 = $ (JD-2450000) $= 6836.0, 6835.17, 6834.73, 6836.45,$
$u_0 = 0.80, 0.82, 0.75, 0.73,$ and
$\chi = 30°.0, -24°.9, -11°.5, 16°.6$; the two parallax amplitude values are $\pi_{E,-} = 0.60$ and $\pi_{E,+} = 1.14$. The corresponding observers' parameters are $u_{0,(1,2)} = 0.87$ and 0.30 with $t_{0,(1,2)} = 6836.36$ and 6829.30 resulting in $\Delta t_0 = -7.1$ day. The "sign" of $u_{0,1}$ is always positive; that of $u_{0,2}$ is negative for two π_E configurations (bottom panels in Figure 1).

Finally, note that in Figure 1 we also indicate the direction of motion. $\Delta t_0 < 0$ results, according to our sign convention, in $t_E > 0$ in the top left and bottom right panels, and $t_E < 0$ in the others.

2.2. Observers in Relative Motion

We now consider the situation for observers in motion. The case of a single observer, specifically the effect of the Earth orbital motion leading to a deviation from the Paczyński shape and its relationship with the microlensing parallax is known (Gould 1992). The first measure of a microlensing parallax due to this effect was reported by the MACHO collaboration (Alcock et al. 1995) to which many additional cases followed whose physical interpretation is not always straightforward (Poindexter et al. 2005). Moreover (and we recall that we are only discussing single-lens systems), the orbital parallax effect becomes observationally relevant only for a minority of unusually long timescale events. For a theoretical analyses of this effect, we also refer to Dominik (1998), Smith et al. (2003), and Gould (2004). Here our goal is to develop the analysis for two observers in motion within the same framework established in Section 2.1. In particular, this will lead us to write a generalization of Equations (2) and (3), relevant for this case.

Within the heliocentric frame, the lens trajectory is always a straight line. The motion of the observer is taken into account by projecting onto the lens plane the temporal evolution of this (known) orbital motion in the ecliptic plane. In the case of a fixed the line of sight, this projection only depends on the microlensing parallax, with a circular orbit being generically projected into an ellipse. In particular, the microlensing parallax is equal to the semimajor axis of the ellipse obtained by the projection of the observer orbit on the lens plane.

The microlensing light curve is determined by the temporal evolution of the lens-observer relative projected distance, $u(t)$, according to the same expression of the magnification $A(t) = A(u(t))$ as in Equation (1), where we now take into account the temporal evolution of the observer position. The combined effect of the two clocks in the system, the unknown microlensing timescale that fixes the velocity of the lens and the known observer orbital motion, means that the resulting light curve will no longer be symmetric around the time at maximum magnification. It is still useful, however, to analyze the configuration in terms of the circle centered on the observer
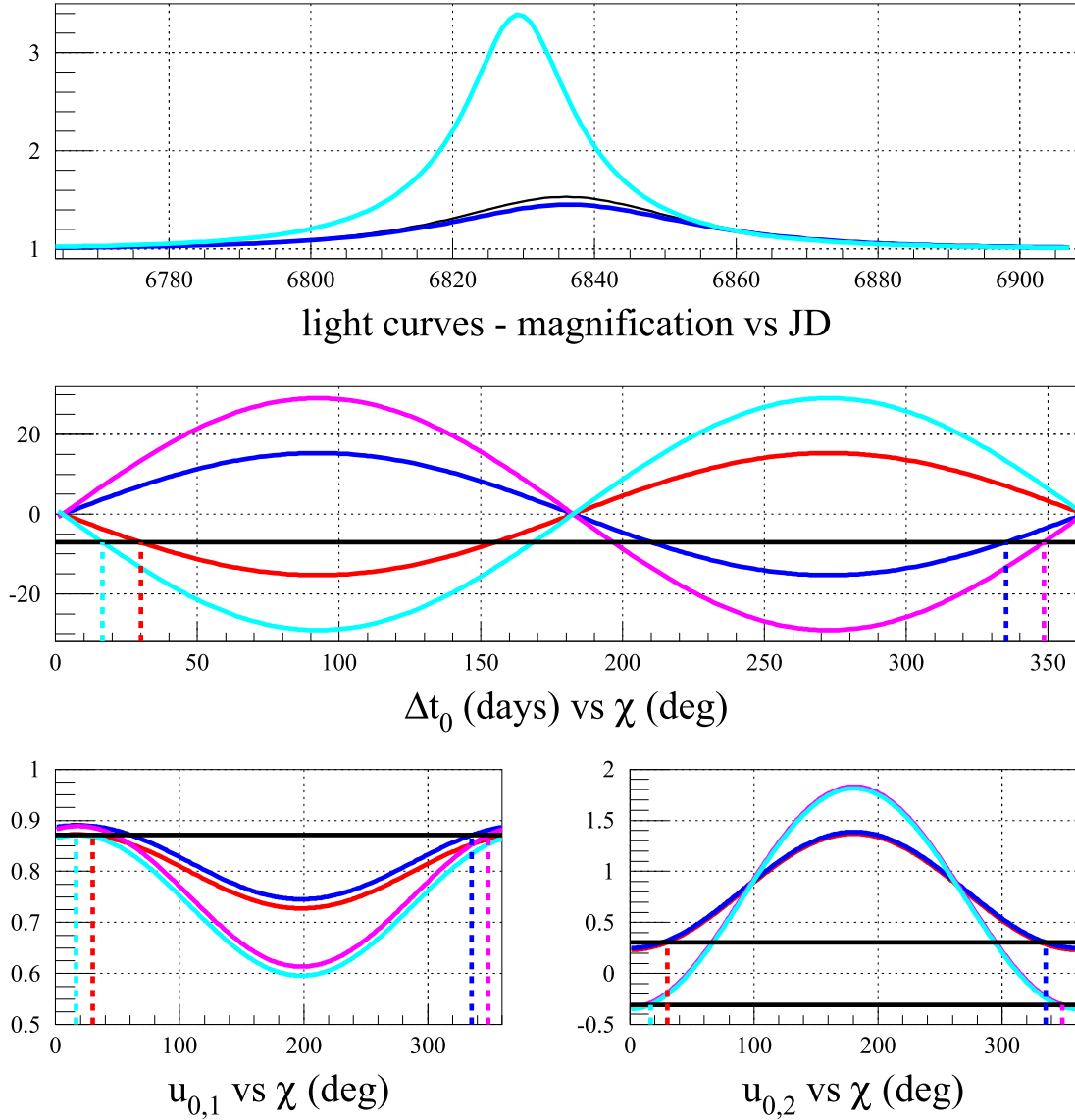
Figure 2. Top panel: the light curves corresponding to the event configurations shown in Figure 1. The thin black line shows one out of four degenerate solutions as would be seen from the Sun, and the dark and light blue curves show the light curves as seen from Earth and *Spitzer*. Middle and bottom panels: the difference of the observers' times at maximum magnification, Δt_0 (middle panel), and observer impact parameters, $u_{0(1,2)}$, for the four degenerate underlying solutions as would be seen from the Sun, as a function of the angle identifying the direction of the lens trajectory, χ. The solid horizontal lines indicate the values for Δt_0 and $u_{0(1,2)}$, corresponding to the case shown in Figure 1, with the vertical dotted lines marking the values of the corresponding angles χ. See Section 2.1 for full details on the event configuration.

position at the time at maximum magnification with radius given by the impact parameter. The specific characteristic for an observer in motion is that this circle is no longer tangent to the lens trajectory, rather, it is secant. Namely, the key point marking out the difference with respect to the case of an observer at rest is that the impact parameter generally does not coincide with the minimum geometrical distance from the observer projected orbital position at the time at maximum magnification to the lens trajectory.

Now we consider two observers in motion. According to the values of the underlying microlensing event, and specifically of the microlensing parallax, we can still find any of the configurations considered in Section 2.1 and shown in Figure 1 as for the relative position of the observers at the time at maximum magnification with respect to the lens trajectory. Additionally, the relative position of the observers still scales

with the microlensing parallax. Accordingly, we can write down an expression similar to Equation (2) where we now have to take into account the effect of the observers' motion

$$\vec{\pi}_{E,\pm} = \frac{\mathrm{au}}{D_\perp} \left(\tau - \Delta u_{0,\parallel}, \; |u_{0,2,\perp}| \pm |u_{0,1,\perp}| \right),$$

$$\Delta u_{0,\parallel} = u_{0,2,\parallel} - u_{0,1,\parallel}$$

$$u_{0,\mathrm{oss},\parallel} = |u_{0,\mathrm{oss}}| \sin(\gamma_{\mathrm{oss}}),$$

$$u_{0,\mathrm{oss},\perp} = |u_{0,\mathrm{oss}}| \cos(\gamma_{\mathrm{oss}}), \quad \mathrm{oss} = 1, 2. \quad (4)$$

Here we introduce the angle γ_{oss} centered on the observer position at the time at maximum magnification, between the orthogonal to the lens trajectory and the line to the intersection of the lens trajectory with the circle of radius $u_{0,\mathrm{oss}}$, so that $u_{0,\mathrm{oss},\parallel}$ and $u_{0,\mathrm{oss}\perp}$ are the projections of the observer impact parameter along and orthogonal to the lens trajectory. In our sign convention, for $t_E > 0$ according to the discussion in

Section 2.1, $\gamma_{\rm oss}$ takes negative (positive) values when $t_{0,\rm oss}$, which is the crossing time of the lens trajectory with the observer circle, comes before (after) the time at the intersection between the lens trajectory and the orthogonal from the circle center. The sign of $\gamma_{\rm oss}$ is then reversed for $t_{\rm E} < 0$. This way $\gamma_{\rm oss}$—independently of the direction of the lens motion and therefore of the sign of $t_{\rm E}$,—always increases anti-clockwise when looking at the lens plane.

Equation (4) reduces to that for the case of observers at rest for $\gamma_{\rm oss} = 0$, namely when the lens trajectory is tangent and not secant as in this case, to the circle centered on the observer position with radius $u_{0,\rm oss}$. Note that the $\gamma_{\rm oss}$ is not an additional free parameter of the problem, rather, it is determined by the interplay within the lens and the orbital motions. As for Equation (2), the components of the parallax vector are meant to be written in a frame with the x-axis parallel to the lens trajectory. Specifically, as for the case of observers at rest, the microlensing parallax is obtained by applying the Pythagoras theorem. The difference comes because τ is (by definition) still equal to the (signed) distance along the lens trajectory between the points of intersection with the observers' circles at the time at maximum magnification, so that the $u_{0,\rm oss,\parallel}$ terms are needed to complete the cathetus delimited by the intersections to the orthogonals from the observer positions to the lens trajectory (in modulus, they can be added or subtracted depending on the sign of $\gamma_{\rm oss}$).

A key point for Equation (4) is that the notation $\pm$ for $\pi_{\rm E,\pm}$ is only meant to describe the two configurations with observers on the same ($-$) or on opposite ($+$) sides of the lens trajectory. However, because of the observers' motion, these are no longer degenerate configurations.

Interestingly, in agreement with Equation (4), it is possible to write an equation relating the relevant lengths along the lens trajectory analogous of Equation (3)

$$\tau - \Delta u_{0,\parallel} = \pi_{\rm E}(\cos(\chi)\Delta y_0 - \sin(\chi)\Delta x_0). \qquad (5)$$

Comparing to the case for observers at rest, on the left-hand side the difference, the new term $\Delta u_{0,\parallel}$, follows from the appearance of the angles $\gamma_{\rm oss}$; however, a key difference is also found in the right-hand side, although formally identical. Now Δx_0, Δy_0, which are the relative observer positions at the time at maximum magnification, are no longer constant (once given the orbit of the observer), rather they depend on all the parameters of the underlying microlensing event configuration, and in particular from χ, and indeed the same holds for the term τ. Therefore this equation no longer identifies degenerate configurations. The underlying motivation is that, as discussed, the observed light curves, fixed the geometrical configuration, depend on the relative lens-observer motion. Any variation in the microlensing parameters is then reflected, in particular, in a change of the observer positions at the time at maximum magnification and ultimately in the light curve observables. In principle, one can invert this line of thought and claim that there is a relationship between the observables, impact parameter, and time at maximum magnification, and in particular the timescale of the underlying microlensing event.

3. ANALYSIS

In the previous sections we revisited the underlying geometrical and mathematical foundations for the description of the measure of the microlens parallax from two distant observers. In particular we noted the differences that arise when moving from the case of observers at rest to that of observers in relative motion, writing down an extension of the Gould (1994) parallax equation that is valid for observers at rest to this case. In this section we first show an example of the configuration described in Section 2.2, then we use specific examples to highlight the importance of fully taking into account the relative motion of the observers for a correct understanding of the underlying microlensing parallax signal.

As above, we consider the case of the simultaneous observation of the same microlensing event from ground and from *Spitzer*. *Spitzer* (Werner et al. 2004) moves along a heliocentric "Earth-trailing" orbit, that is currently at a distance of about 1 au from Earth.[7] For simplicity, we approximate both Earth's and *Spitzer*'s orbits as circular, with radius 1 au and a constant angular velocity with a period of 1 year and 373 day, respectively. We fix the Earth and *Spitzer* phases, their relative azimuthal angles, at the time of the autumnal equinox. For 2014, at JD-2450000 $= 6923.6$, $\Delta\lambda = -79^\circ\!.7$.

In Figure 3 we show a specific two-observers microlensing parallax configuration on the lens plane. The analysis is carried out following the discussion in Section 2.2. In particular, we evaluate the observers' impact parameters and time at maximum magnifications through a numerical minimization of the function $u(t)$, taking into account both the lens and the observers' orbital motion. The ellipse indicates the projection of the Earth and *Spitzer* orbits on the lens plane. The dotted points along the trajectories are equally spaced by 5 day, with empty symbols for times prior t_0, showing the direction of motion. We note, as discussed in Section 2.2, that the lens trajectory is *secant* to the two circles of radius $u_{0,\rm oss}$ centered on the orbital positions at time $t_{0,\rm oss}$ (and no longer tangent as for the case of observers at rest; Figure 1). For reference, the microlensing event configuration is as follows. The line of sight toward the Bulge is fixed at R.A., decl. $= 266^\circ\!.8, -21^\circ\!.4$ (we see here a generic feature of the *Spitzer* observational campaign in 2014 and 2015, with Earth and *Spitzer* almost aligned along the equatorial axis). The microlensing event parameters are $t_0 = ({\rm JD}-2450000) = 6836.0$, $u_0 = 0.4$, $t_{\rm E} = 28.5$ day, $\chi = 45^\circ$, and $\pi_{\rm E} = 0.76$, which results in a $\pi_{\rm E,+}$ configuration and observers on different sides of the lens trajectory with $u_{0,(1,2)} = 0.47, 0.15$ and $t_{0,(1,2)} = 6831.5, 6821.2$ with $\Delta t_0 = -10.3$ day. Comparing with the case of observers at rest there is now, in agreement with Equation (4), a non-zero value for $\gamma_{\rm oss}$ with $\gamma_{1,2} = -20^\circ$ and 2° (note in particular the negative sign of γ_1). As further detailed below, it is useful to estimate a proxy for the event timescale analog to the Einstein time for the observed light curves. In this case it results in $t_{e,oss}$ equal to 36 and 29 days, respectively.

In Figure 4 we show, top panel, the light curves for the microlensing event shown in Figure 3 as would be seen from the Sun, and those for the Earth and *Spitzer* observers. In the middle and bottom panels we show a few characteristic quantities for this microlensing event configuration by varying the angle χ. In particular, we show Δt_0 and $u_{0,\rm oss}$, which are no longer symmetric as in the case with observers at rest (Figure 1). Furthermore, we show the characteristic quantities for observers in motion: the angle $\gamma_{\rm oss}$, which we see can becomes rather large, and the estimated timescale along the

---

[7] The ephemeris of *Spitzer* as a function of time can be found on the NASA-JPL Horizon system http://ssd.jpl.nasa.gov/?horizons.
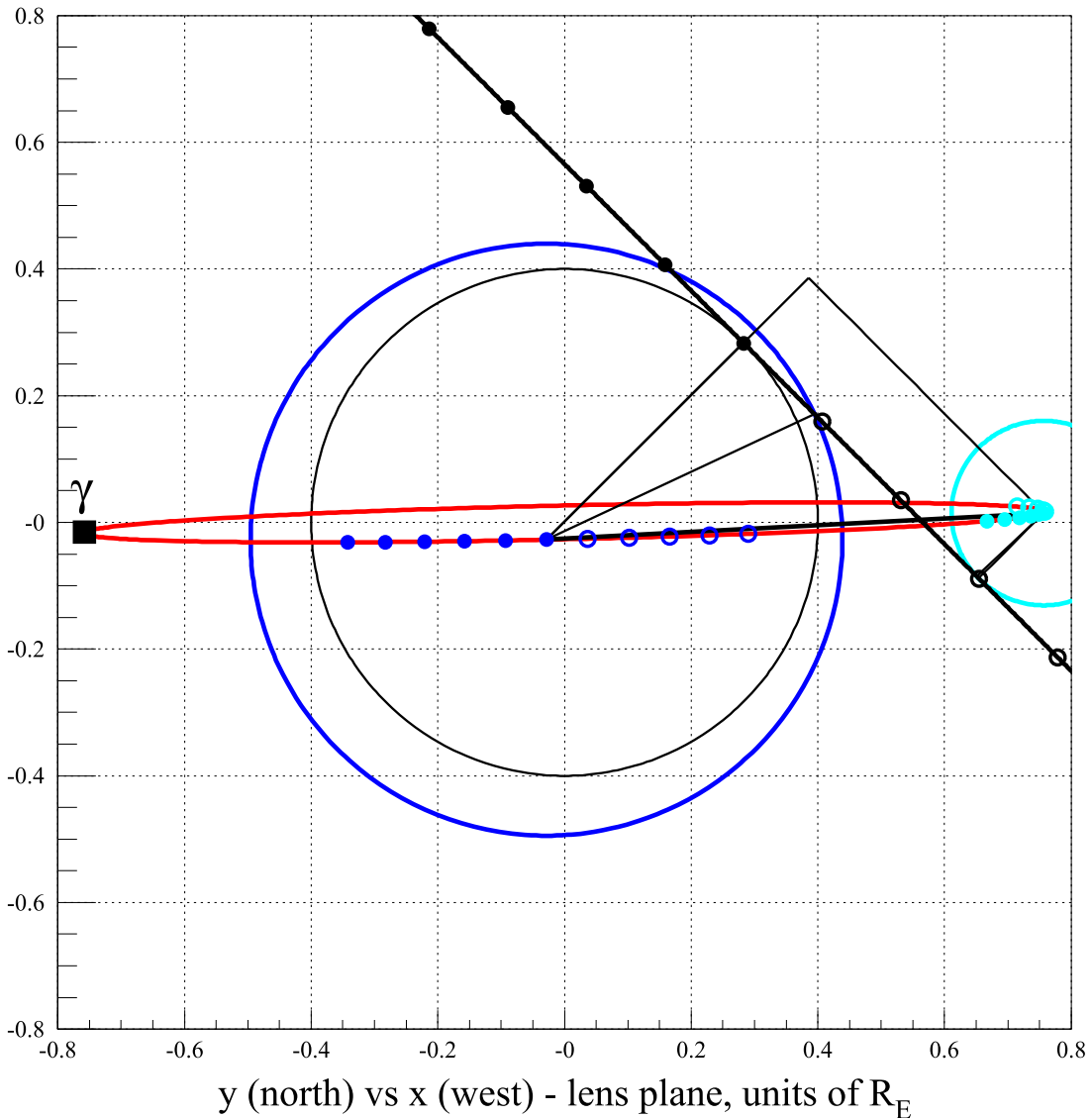
Figure 3. Projected in the lens plane, in a heliocentric reference frame centered on the line of sight to the source, the configuration for a parallax microlensing event for two observers in motion on Earth and *Spitzer* for a line of sight toward the Bulge (see Section 2.2 for full details). The thin black circle is centered on the origin, radius the impact parameter as would be seen from the Sun. The thick circles are centered on the observer positions at the times of their respective maximum magnification, with a radius of their respective impact parameters, dark and light blue for Earth and *Spitzer*. The red elongated ellipse represents the projected orbit of the observers (the square indicates the position of the Earth at the fall equinox). The thick straight line tangent to the circle of radius u_0 and secant to the observer circles is the lens trajectory. The dots along the trajectories are equally spaced by five days, with empty ones for times prior the respective times at maximum magnification. The centers of the Earth and *Spitzer* circles are joined by a thick line whose length scales with the microlensing parallax; the thinner lines indicate the triangle construction underlying Equation (4). The reference frame is as in Figure 1.

observers' light curves, $t_{E,oss}$. Note that, in addition to $u_{0,oss}, \gamma_{oss}$ is also shown to taking into account the sign of the configuration as defined in Section 2.1. An inspection of the bottom right panel reveals that the $t_{E,oss}$ values can be significantly different from one another, and from the duration of the underlying microlensing event, t_E. Indeed, also comparing to Figure 3, we see that the larger differences for $t_{E,1}$ from t_E occur for a lens direction of motion along the *x*-axis. This is caused by the Earth's position along its orbit at the time at maximum magnification, with the relative lens-observer velocity getting to a minimum (maximum), and correspondingly the duration of a maximum (minimum) for values about $\chi = \pi/2 \ (3\pi/2)$, respectively.[8]

In Section 2.2 we discussed the underlying reason why the microlensing parallax degeneracy is broken once introduced in the observer motion. However, one may assume that the deviations from the case with observers at rest are "small" and look also in this case for the analog of the degenerate configurations discussed with observers at rest. More specifically, the ratio of the analysis is the following. For a given set of parameters we evaluate, following the analysis in Section 2.2, the microlensing light curves as seen by the observers in motion, and in particular the values for the impact parameter and time at maximum magnification, are $(u_0, t_0)_{oss}$. We then consider as given these values, fix the positions of the observers along their orbits at their respective time at maximum magnification, and, following the analysis in Section 2.1, study the event under the assumption of observers at rest, namely
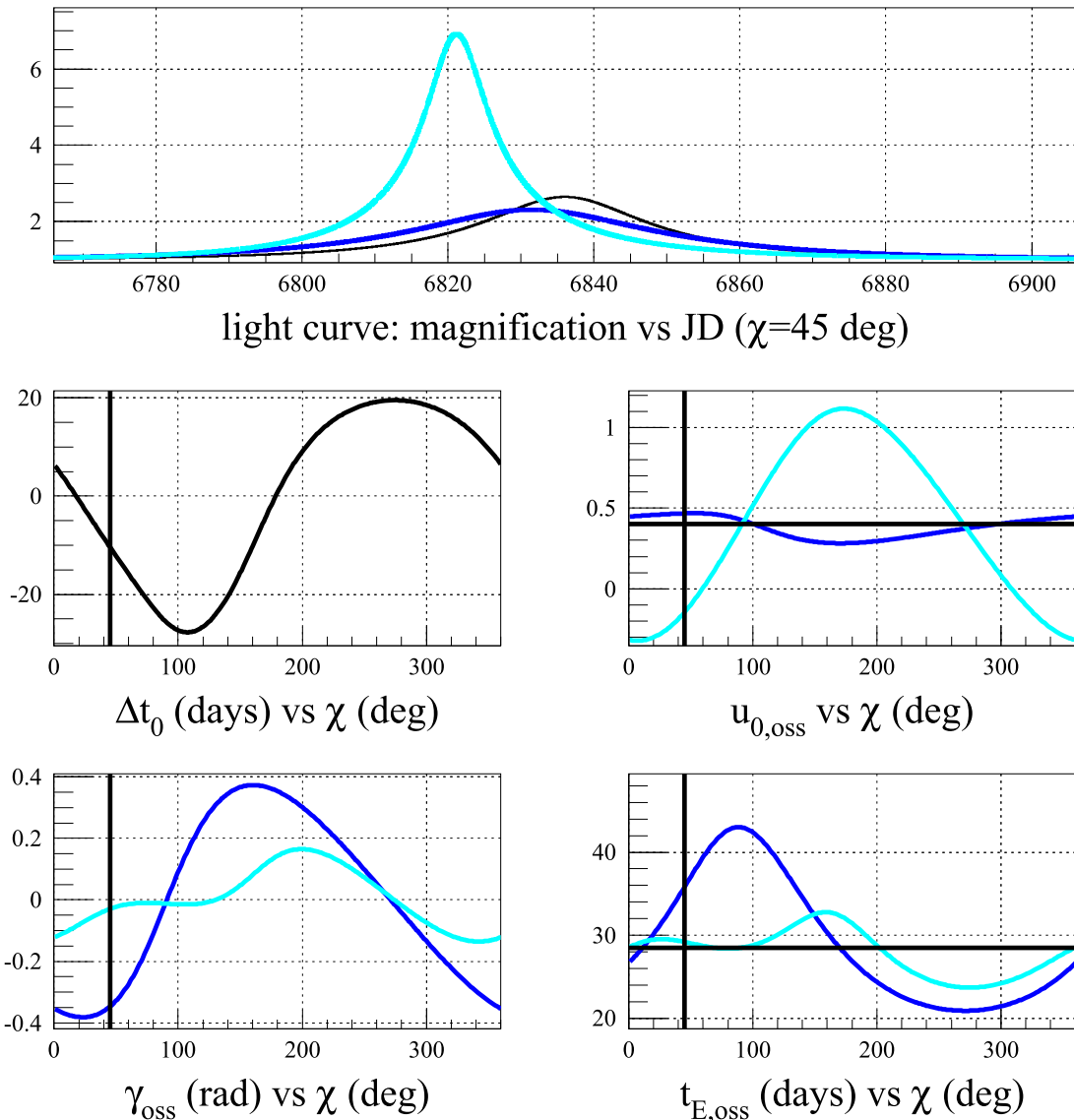
---

[8] Our sign convention for t_E, as also apparent from Figure 3, is the same as in Section 2.1.

Figure 4. Top panel: the light curves for the microlensing event configuration shown in Figure 3. The thin black line is for the event as seen from the Sun; the dark and light blue lines show the light curves as seen from Earth and from *Spitzer*. Middle and bottom panels: for the same event configuration, varying the angle χ of the direction of the lens trajectory, with a difference of time at maximum magnification, Δt_0, observers' impact parameters, $u_{0,oss}$, angle γ_{oss}, and duration for the observers' light curves, $t_{E,oss}$. The vertical lines indicate the value for χ used for the light curves in the top panel, the horizontal lines show the values u_0 and t_E of the underlying microlensing event as seen from the Sun.

through Equations (2) and (3). Specifically, in the analysis we evaluate the microlensing parallax and the observable quantities and compare them to the "true" values as in the original configuration with observers in motion.

Additionally, we consider the observed timescale, which is key to addressing the issue of the breakdown of parallax degeneracy. Indeed, Gould (1995) acknowledged that the microlensing parallax fourfold degeneracy is broken as soon as one drops the assumption of observers at rest, and in particular remarked that the two observers (from the ground and from the satellite) would measure a different timescale. Gould (1995) then derived a relationship (his Equation (2.3)) for evaluating the difference of the observed parameters given the relative motion of the observers, and all in principle directly observable quantities: the timescale difference (rather, $\Delta\omega$, the difference of the inverse of the timescale, $\omega = 1/t_E$), and the difference of the times at maximum magnification. This same equation

then became the basis to address the issue of the possibility of breaking the degeneracy for the analyses by Boutreux & Gould (1996) and Gaudi & Gould (1997), with the simulation of parallax microlens events toward the Magellanic Clouds and the Galactic bulge, respectively.

From the standpoint of our analysis in Section 2.2, considering in particular Equation (4), it is relevant to observe that the analysis in Gould (1995) is still based on Equation (2), which is valid for observers at rest. Looking at the relationship obtained by Gould (1995) as an equation for $\Delta\omega$, we may therefore compare this "expected" value to the "true" one, which we can estimate from the analysis of the light curves. This way we can test whether the estimate is reliable for assessing the breaking of the degeneracy.

Before moving onto presenting the results of this analysis, we first note what we intend by "timescale" for the case of observers in motion. The Einstein time, t_E, as appears in

Equation (1), is well-defined for a light curve symmetric around the time at maximum magnification, t_0, and in particular it results that the magnification $A(t)$ for $t = t_E$ is that evaluated for a value $u(t) = \sqrt{u_0^2 + 1}$. As detailed above, the light curve for observers in motion is no longer symmetric and by itself is a single parameter because the timescale, however defined, cannot grasp both the width of the light curve and the degree of asymmetry. Still, it remains a useful indicator of the light curve shape. Based on the definition valid for an observer at rest, and as a proxy for the timescale for observers in motion, we proceed as follows. Given the observable $u_{0,\text{oss}}$, we evaluate the value of the magnification of a hypothetical Paczyński light curve with this value for the impact parameter at the time corresponding to that of the Einstein time, which we call $\bar{A}$. Moving back to the observed light curve, we numerically evaluate the time interval, which is in general asymmetric around the time at maximum magnification, fixed by the intersection of the light curve with the value $\bar{A}$, and define the "Einstein time" for the observer in motion, $t_{E,\text{oss}}$, as half this interval (with the true t_E being therefore recovered for a symmetric light curve).

We fix the line of sight toward the Bulge and t_0 as in Figures 1 and 2. With the lens mass fixed at $0.6\,M_\odot$, we consider two cases: a lens in the Disc at $D_l = 2.0$ kpc and a lens in the Bulge at $D_l = 7.5$ kpc. For $D_s = 8$ kpc this gives $\pi_E = 0.28$ and 0.04, respectively. For $v = 300$ and $80\,\text{km s}^{-1}$, the timescale is 16 and 59 day for the disc lens, and 8.7 and 33 day for the bulge lens. In Figures 5 and 6 (bulge and disc lens, respectively) we show as a function of the angle of the lens motion χ for two values of the impact parameter, $u_0 = 0.1$ and 0.8 (from top to bottom, for increasing impact parameter and event duration), the values for $u_{0,\text{oss}}$; the horizontal solid line indicates u_0 for the Sun observer, those for $\pi_{E,\Delta\pm}$ as calculated for observers at rest, where the solid horizontal line indicates the true value for π_E, and $\Delta\omega$ corresponding to $\pi_{E,\Delta\pm}$. Note that the two degenerate solutions for the parallax amplitude, and correspondingly the values for $\Delta\omega$, are evaluated based on $\Delta_\pm \equiv \Delta u_{0,\pm} = u_{0,2} \pm u_{0,1}$, namely taking into account the sign of $u_{0,\text{oss}}$. This way the Δ_- solution always has the same parity of the original configuration, $\pi_{E,-}$ or $\pi_{E,+}$ (with the changes between the parity following the sign of $u_{0,\text{oss}}$). Indeed, we can see that the $\pi_{E,\Delta-}$ solution always remains close enough to the true value, whereas $\pi_{E,\Delta+}$ can get quite different. Interestingly, however, there are also ranges of χ values for which $\pi_{E,\Delta+}$ can get closer to the true value than $\pi_{E,\Delta-}$, so that in principle the analysis based on the assumption of observers at rest may lead to the correct value for π_E, although with the wrong sign of the parity. In general we see that a larger value of u_0 or t_E increases the difference between the $\pi_{E,\Delta-}$ and $\pi_{E,\Delta+}$ values and the relative difference with respect to the true value π_E, as well as increasing the difference between $\Delta\omega$ calculated for observers at rest with respect to the true value. However, while these differences do not become really significant for the bulge lens, so that the lens motion may indeed be neglected in the analysis, this is no longer true for the disc lens configuration. It is apparent, therefore, that aside from the effect of the direction of motion, larger values of the microlens parallax (for large enough u_0) and therefore for decreasing values of the lens mass and nearer lenses, tend to enhance the importance of the observers' motion. This effect is balanced by the event duration, which decreases both with lens mass and the lens distance.

4. K2 AND SPITZER PARALLAX: A THREE OBSERVERS PROBLEM

In spring 2016, K2 (Howell et al. 2014), the extension of the *Kepler* (Borucki et al. 2010; Koch et al. 2010) mission, is expected to carry out a three-month microlensing monitoring toward the Galactic bulge during its K2C9 campaign, which is the first space-based microlensing survey ever (Henderson et al. 2015). The K2 survey mode of operation is opposed to that of the *Spitzer* observational program, which monitors microlensing events in a follow-up mode (Yee et al. 2015a). This will allow K2 to address several relevant scientific questions related to the observation of a typology of microlensing events, such as high magnification and/or short timescale ones, which are likely to be missed by *Spitzer*.

Kepler is moving along an Earth-trailing orbit similar to that of *Spitzer*, which we approximate in a similar way as in Section 2.2 (the exact ephemeris can be found on the NASA-JPL Horizon system). We fix the phase shifts at the fall equinox 2016, JD-2450000 = 7654.1, for *Spitzer* and K2 at $\Delta\lambda = -94^\circ.4, -52^\circ.7$, respectively.

K2C9 is going to last about three months, starting 2016 April, so this observational period will (partly) overlap with that of the expected 2016 *Spitzer* follow-up microlensing project that is expected to start in 2016 June (this campaign must obey the *Spitzer* visibility constraints toward the Bulge). For the first time it will be possible to simultaneously observe the same microlensing events from the ground and two satellites in orbit. This is relevant to our analysis because, within the framework of observers at rest, the fourfold degeneracy is broken by the introduction of a third observer, an effect that is enhanced when correctly taking into account the motion of the observers. However, it is interesting to address this issue within the framework of observers at rest to appreciate the extent to which the degeneracy is actually broken. From an inspection of Equation (3), we see that the difference between the times at maximum amplification is going to be different for K2 and *Spitzer*, so that the respective degenerate solutions for the lens trajectory are going to be different. Equation (2) then implies that the difference in the impact parameters will determine two different sets of $\pi_{E,\pm}$ solutions, thus giving the chance, when analyzed together, to single out the correct one (recall that the degeneracy breaking for K2 microlens parallaxes is the specific purpose of one of the accepted proposals (Gould et al. 2015a) for the forthcoming 2016 *Spitzer* campaign).

This is exemplified in Figure 7, where we show the configuration in the lens plane for the three observers' case for a specific microlensing event configuration and four test values of the lens trajectory. We show the circles of radius $u_{0,\text{oss}}$ centered on the observers' positions (here considered at rest, as evaluated at $t = t_0$) and the lens trajectory that is now simultaneously tangent to all three observer circles. At a glance it is clear that, when considering both couples of observers simultaneously, the degeneracy for the parallax vector directions and amplitude is broken. For reference, we fix the line of sight to that expected to be the center of K2C9 field, R.A., decl. $= 270^\circ.354, -21^\circ.780$. We fix $t_0 = (\text{JD-2450000}) = 7561$ (2016 June 21), $u_0 = 0.5$, $t_E = 24$ day, $\pi_E = 0.8$, and test four values for the angle of the lens trajectory (top to bottom, left to right) $\chi = 15^\circ, 30^\circ, 45^\circ$ and 60°. The resulting u_0 from ground is always about 0.52–0.53, for *Spitzer* 0.28, 0.20, 0.078, and 0.084, and for
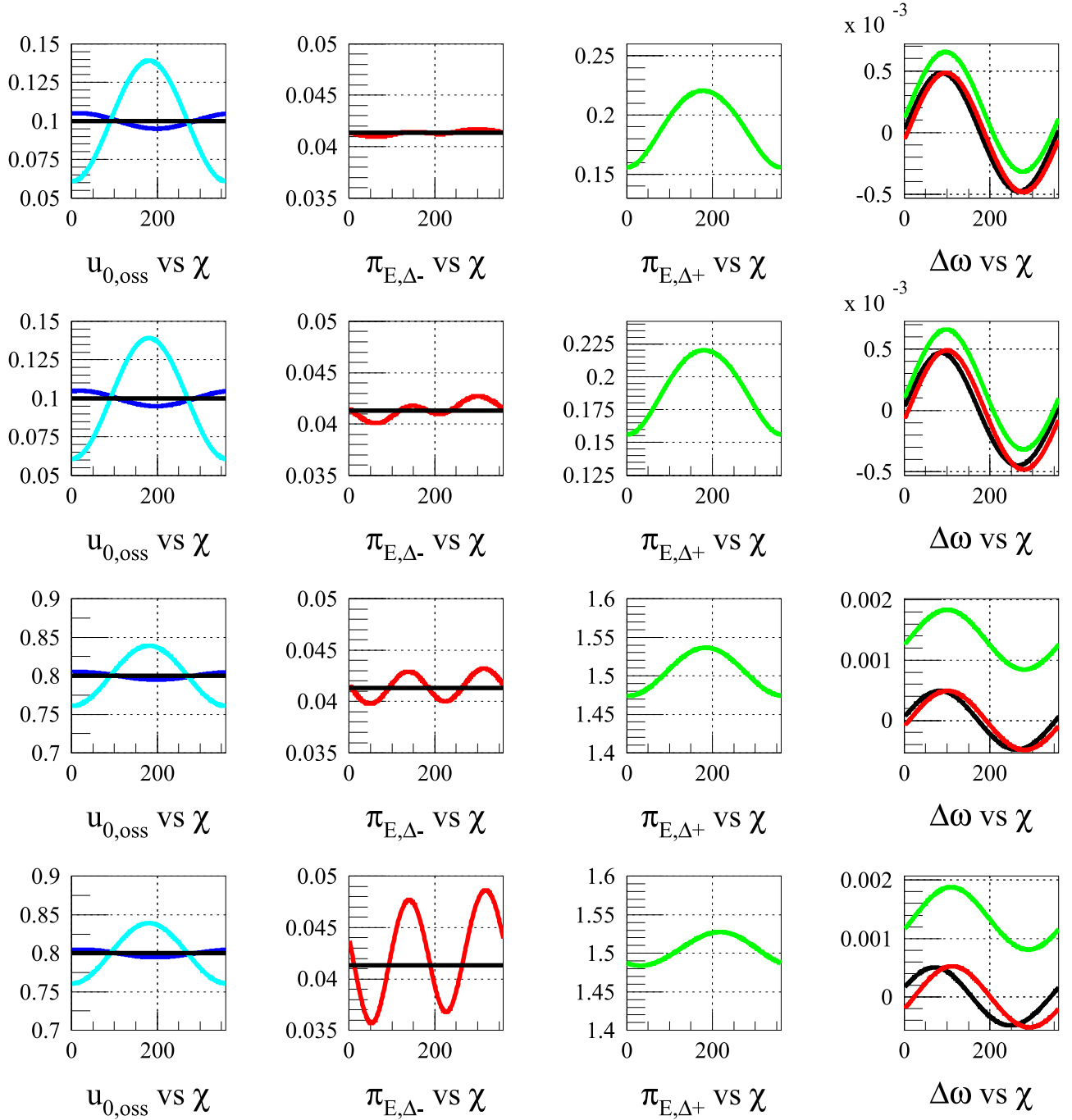
Figure 5. We show for a Bulge lens, as a function of the direction of the the lens trajectory, angle χ expressed in degree, from left to right, $u_{0,oss}$, as evaluated for observers in motion, and the corresponding values as evaluated assuming observers at rest for $\pi_{E,\Delta\pm}$ and $\Delta\omega$. The true value is in black, and red and green correspond to $\pi_{E,\Delta\pm}$. The solid horizontal lines for u_0 and π_E indicate, respectively, the impact parameter as would be seen from the Sun and the value of the microlens parallax for the underlying microlensing event. From top to bottom we show different configurations increasing the value of the impact parameter and the event duration. We refer to Section 3 for full details.

K2 0.087, 0.025, 0.073, and 0.2; Δt_0 is -4.0, -8.8, $-13.$, $-16.$ days for *Spitzer* and -3.3, -7.0, -10 and -13 days for *K2*, respectively. The degenerate directions for each couple, Earth–*Spitzer* and Earth–*K2*, are clearly different. The resulting degenerate values of the parallax amplitude are different as well. In particular (for a true value $\pi_E = 0.8$) for *Spitzer* and *K2* we evaluate 0.29 and 0.59 ($\chi = 15°$), 0.48 and 0.74 ($\chi = 30°$), 0.69 and 0.94 ($\chi = 45°$), and 0.90 and 1.15 ($\chi = 60°$), so that for this configuration the degenerate solution shifts from $\pi_{E,-}$ to $\pi_{E,+}$ at $\chi = 45°$ for *K2* and at

$\chi = 60°$ for *Spitzer*. Clearly, the degree by which the degeneracy is broken can be measured by how much the degenerate solutions, in term of direction or of the amplitude of $\vec{\pi}_E$, differ from one another when simultaneously considering the two couples of observers. Hereafter we focus on the amplitude of the microlensing parallax.

For the analysis of Figure 7, we considered the respective positions of the observers along their orbit, specifically given their (fixed) phase shift. This is a relevant aspect that leads us to discuss the seasonal effects for the measure of the microlens
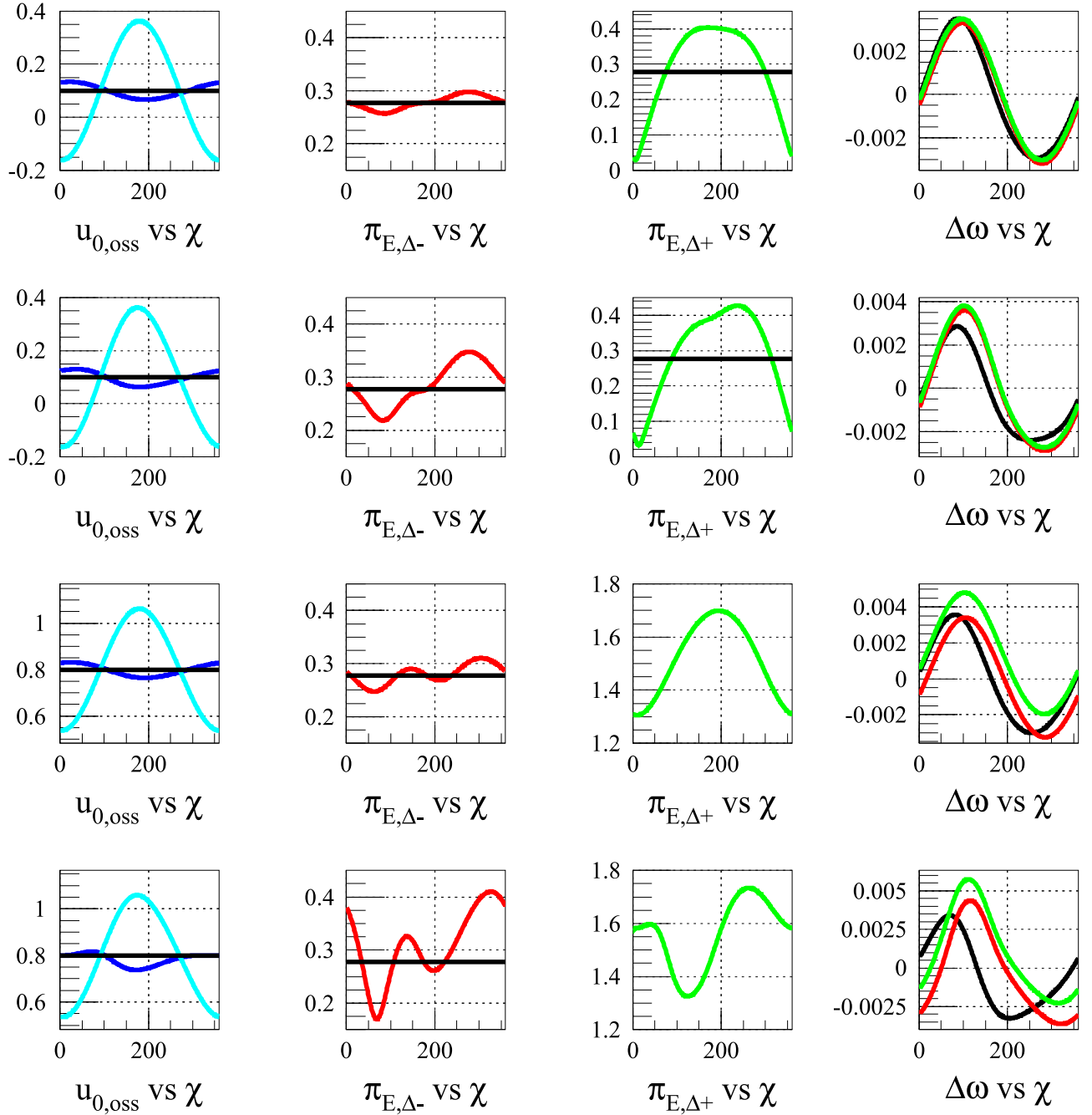
Figure 6. The same as in Figure 5, here for a lens in the Disc. We refer to Section 3 for full details.

parallax for two observers lying along the ecliptic plane. Indeed, the line of sight toward the Bulge is near the ecliptic plane, and therefore the projection on the lens plane of the distance between the two observers (which remains roughly constant on the ecliptic plane along the few months of a given observation campaign) is a strong function of the period of the year. This is relevant because, from Equation (2), we see that $\pi_E \propto 1/D_\perp$. All the microlensing parameters remain fixed, in particular the parallax, whenever $D_\perp$ becomes very small, namely when the two observers are roughly aligned with the line of sight toward the Bulge, and the larger we can expect the degenerate parallax solution to be. On the other hand, $\pi_E \propto \sqrt{1/M_l}\sqrt{(1-x)/x}$, so that large values for π_E are expected for very small lens mass or very nearby lenses. Values

that are too extreme (at least for lenses in the stellar mass range), roughly $\pi_E > 2$, are however by themselves extremely unlikely.

In Figure 8 we show the variation of the degenerate parallax solution, $\pi_{E,2}$ (which can be $\pi_{E,-}$ or $\pi_{E,+}$) as a function of the time of the year, $\bar{t}$. Specifically, we fix the underlying microlensing event configurations with the time at maximum magnification, as seen from the ideal observer on the Sun, at $t_0 = \bar{t}$. At the same time, we fix the positions along the orbit of the three observers—Earth, *Spitzer* and *K2*—at $t_0 = \bar{t}$. In particular, given the line of sight, the direction of the lens motion, and the event timescale, we show the results for different combinations of the impact parameter and the microlens parallax. For reference, the line of sight is fixed as
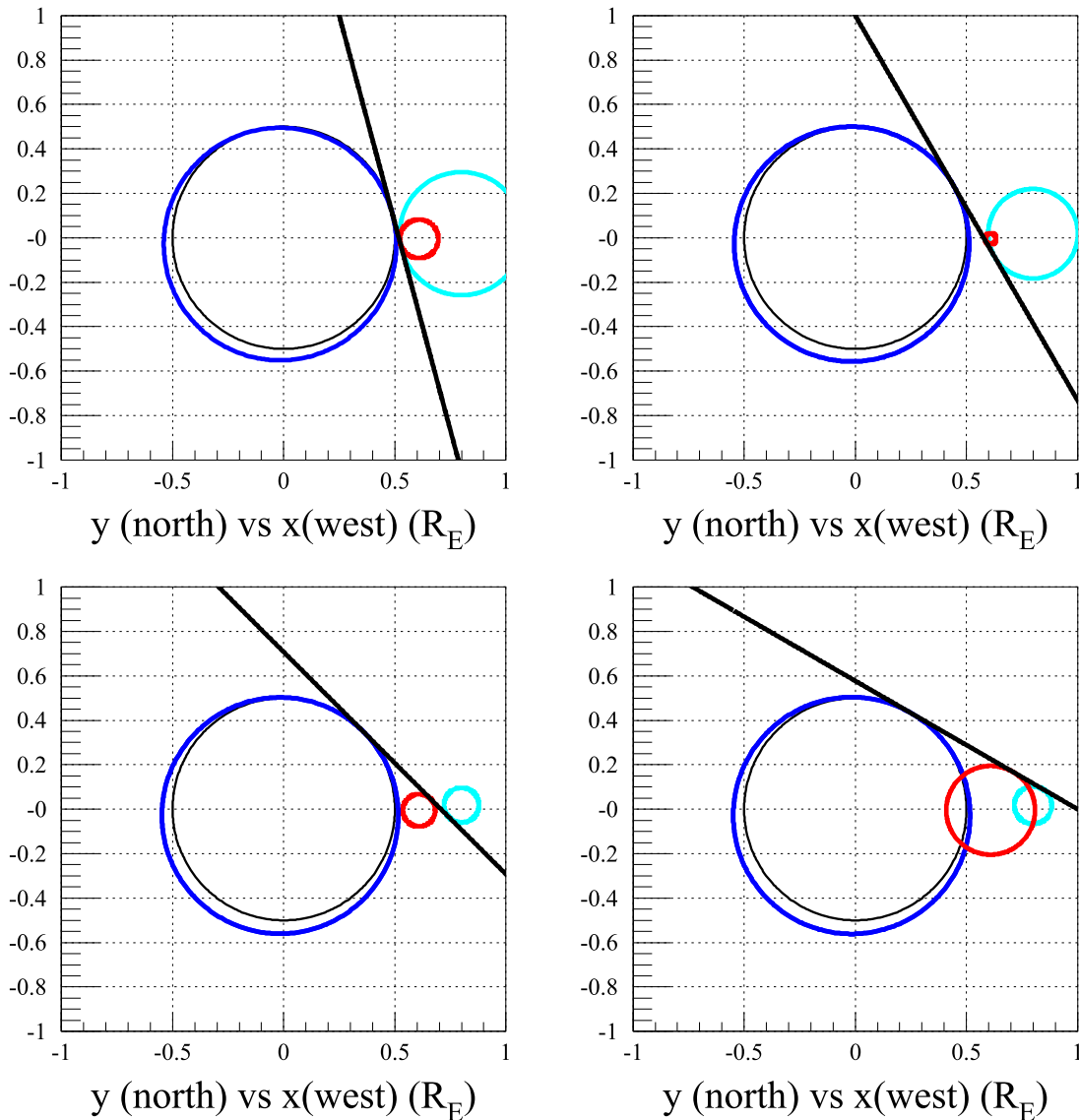
Figure 7. The configurations for four different lens trajectories, for a parallax microlensing event for three observers at rest, Earth, *Spitzer* and *K2*, for a line of sight toward the bulge projected in the lens plane in a heliocentric reference frame centered on the line of sight to the source (see Section 4 for full details). The thin black circle is centered on the origin, radius the impact parameter as would be seen from the Sun. The thick circles are centered on the observer positions, with radius the respective impact parameters; the dark blue, light blue, and red circles are for Earth, *Spitzer*, and *K2*. The straight line represents the lens trajectory, which is simultaneously tangent to all the circles. The reference frame is as in Figure 1.

for the events shown in Figure 7, $t_E = 24$ day and $\chi = 30°$. We then test two values for the microlens parallax, $\pi_E = 0.01$ (two top panels) and $\pi_E = 1.3$ and two values for the impact parameter, $u_0 = 0.01$ (top to bottom, first and third panels) and $u_0 = 0.8$. We can see that the difference in the orbital phase shift between *Spitzer* and *K2* introduces a shift in the peak for $\pi_{E,2}$ and that, besides $\bar{t}$, the underlying microlensing configuration also plays a relevant role, even leading to rather wild variations. Focusing in particular on 2016 June, starting about JD-2450000 = 7550 when the *Spitzer* and *K2* campaigns will overlap, we see that regardless of the microlens parallax value, small values for the impact parameter tend to smooth over the difference between the $\pi_{E,2}$ values as seen by *Spitzer* and *K2*, whereas larger values for u_0 quickly lead to a rather large offset between the two $\pi_{E,2}$ values, which can therefore resolve the parallax degeneracy. Finally, we note that for *Spitzer*, within the boundaries of the observational window, $\pi_{E,2}$ tends to

remain roughly constant, or in any case bounded to smaller value, which is not the case for *K2*.

5. CONCLUSION

In this work we revisited the analysis of the microlensing parallax for the case of a simultaneous observation of the same microlensing event by two and three observers (Refsdal 1966; Gould 1994) from within an heliocentric frame. The main purpose of this analysis is the understanding of the fourfold microlensing parallax degeneracy and of how it is broken. First we discussed the case for observers at rest and went through the geometrical meaning of the microlensing parallax degeneracy, in particular we explicitly detailed an expression for the degenerate directions of the lens trajectory as a function of the microlensing parallax, π_E, and $\tau = \Delta t_0/t_E$ only. Second, we considered the case for observers in motion and devised an extension to this case of the Gould (1994) relationship between
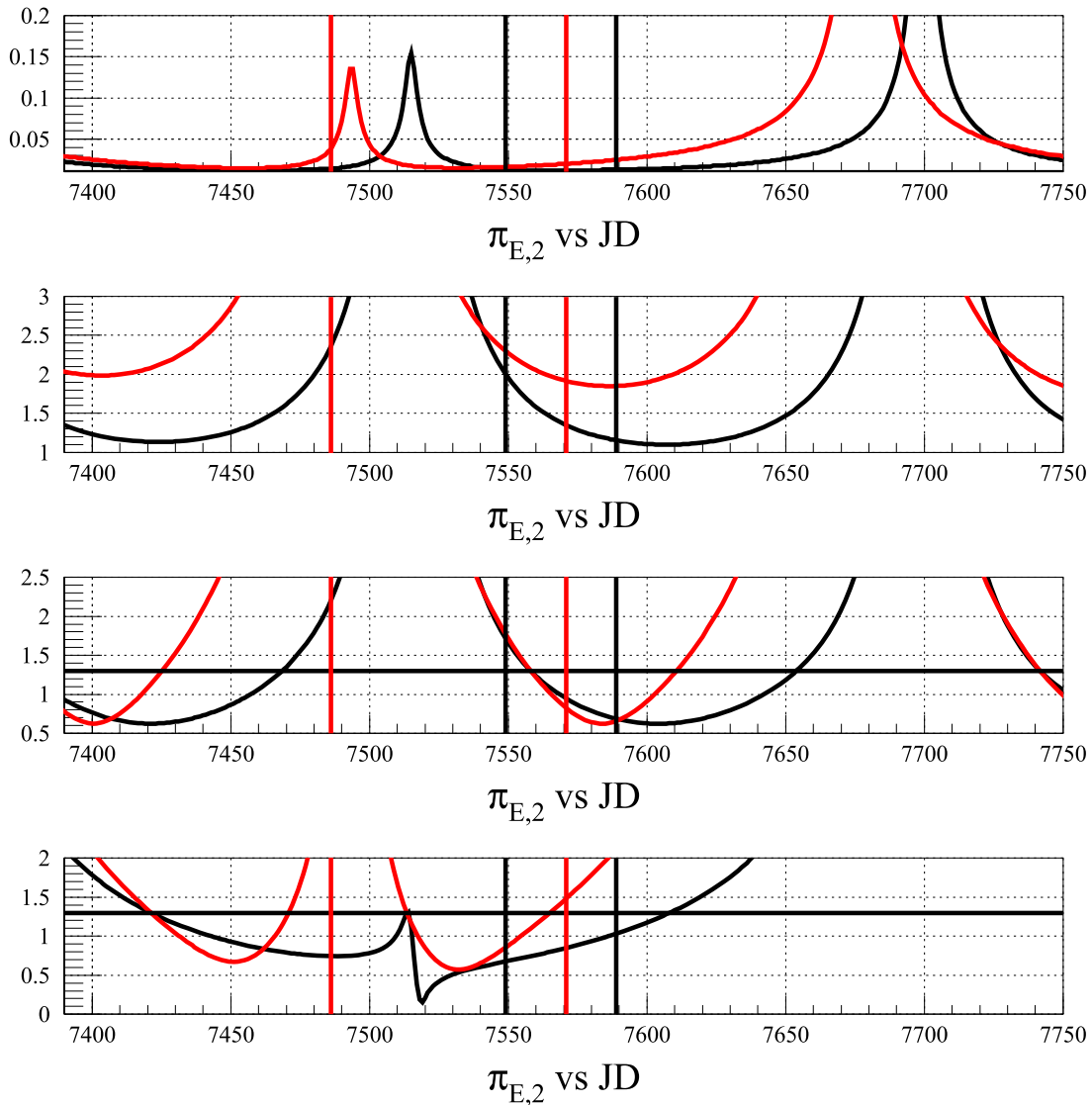
Figure 8. The degenerate value of the amplitude of the microlens parallax, $\pi_{E,2}$, for a given event configuration as a function of the time at maximum magnification fixed at the date of the day of the year 2016, as measured from *Spitzer* and *K2* (black and red lines) observers at rest. The horizontal lines indicate the true value of the amplitude of π_E. The two top (bottom) panels for $\pi_E = 0.01$ (1.3), first and third (second and fourth) panels from top for $u_0 = 0.01$ and 0.8, respectively. The vertical lines delimit the 2016 *Spitzer* and *K2* campaigns. We refer to Section 4 for full details.

the microlensing parallax and the light curve observables. We discussed how the geometry of the microlensing parallax configuration is now determined by the parameters of the underlying microlensing event, in particular the duration, which is the underlying reason for the break down of degeneracy in this case. Throughout the analysis, the choice of a heliocentric reference frame allowed us to get a clear geometrical and analytical insight.

As test case we considered simultaneous observations from the ground and *Spitzer*, which are relevant in consideration of the ongoing follow-up observational campaign toward the Galactic Bulge (Gould et al. 2013, 2014, 2015a, 2015b). The analysis, through a series of test cases, hints that the motion of the observers can be expected to be relevant, especially for disc lenses with large enough impact parameters and a long enough timescale. These are the cases, therefore, for which one may expect to be able to more easily break the degeneracy from an observational point of view.

Finally, we discussed the case for three simultaneous observers, relevant for the foreseen *K2* microlensing survey expected for 2016, which will also partly overlap with the *Spitzer* season. In this case, the microlensing parallax degeneracy is already broken from the standpoint of an analysis based on the assumption of observers at rest. Through a series of test cases we have shown how this can be actually effective.

In this work we explicitly have not addressed the issue of the actual determination of the microlensing parameters out of observed light curves. As a standard, for instance for the analysis of the *Spitzer* light curves (Calchi Novati et al. 2015a), the scheme developed by Gould (2004) from within a geocentric frame is used. A drawback of this approach is that in the end, one has to come back to the heliocentric frame to determine some parameters, notably the event duration. A main advantage, however, is that the observed underlying event parameters, time of maximum magnification, impact parameter, and duration, are similar to those that can be estimated from the

NOVATI & SCARPETTA

ground in absence of the parallax effect. In principle, however, this is exactly where the simultaneous observations from a space observer may help. With reference to the *Spitzer* campaign, however, we recall that even when the problems related to the determination of the source flux and the different blend fractions are put aside, the limited baseline in most cases does not allow us to fully independently characterize the microlensing light curve. This represents a major problem for the practical application of the analysis presented in this work, and holds in particular for the case of the three observatories. Still, it will be interesting to analyze the *K2* data, which, thanks to the survey mode and longer baseline available, may be expected to suffer less from this limitation.

REFERENCES

Alcock, C., Allsman, R. A., Alves, D., et al. 1995, ApJL, 454, L125
Batista, V., Beaulieu, J.-P., Bennett, D. P., et al. 2015, ApJ, 808, 170
Bennett, D. P., Bhattacharya, A., Anderson, J., et al. 2015, ApJ, 808, 169
Borucki, W. J., Koch, D., Basri, G., et al. 2010, Sci, 327, 977
Boutreux, T., & Gould, A. 1996, ApJ, 462, 705
Calchi Novati, S., Gould, A., Udalski, A., et al. 2015a, ApJ, 804, 20
Calchi Novati, S., Gould, A., Yee, J. C., et al. 2015b, ApJ, 814, 92
Dominik, M. 1998, A&A, 329, 361
Dong, S., Udalski, A., Gould, A., et al. 2007, ApJ, 664, 862
Gaudi, B. S., & Gould, A. 1997, ApJ, 477, 152
Gould, A. 1992, ApJ, 392, 442
Gould, A. 1994, ApJL, 421, L75
Gould, A. 1995, ApJL, 441, L21
Gould, A. 1997, ApJ, 480, 188
Gould, A. 1999, ApJ, 514, 869
Gould, A. 2000, ApJ, 542, 785
Gould, A. 2004, ApJ, 606, 319
Gould, A. 2013, ApJL, 763, L35
Gould, A. 2014, JKAS, 47, 215
Gould, A., Carey, S., & Yee, J. 2013, Spitzer Microlens Planets and Parallaxes, Spitzer Proposal
Gould, A., Carey, S., & Yee, J. 2014, Galactic Distribution of Planets from Spitzer Microlens Parallaxes, Spitzer Proposal
Gould, A., Yee, J., & Carey, S. 2015a, Degeneracy Breaking for K2 Microlens Parallaxes, Spitzer Proposal
Gould, A., Yee, J., & Carey, S. 2015b, Galactic Distribution of Planets From High-Magnification Microlensing Events, Spitzer Proposal
Gould, A., Udalski, A., An, D., et al. 2006, ApJL, 644, L37
Henderson, C. B., Park, H., Sumi, T., et al. 2014, ApJ, 794, 71
Henderson, C. B., Penny, M., Street, R., et al. 2015, PASP, submitted (arXiv:1512.09142)
Howell, S. B., Sobeck, C., Haas, M., et al. 2014, PASP, 126, 398
Koch, D. G., Borucki, W. J., Basri, G., et al. 2010, ApJL, 713, L79
Mao, S. 2012, RAA, 12, 947
Paczyński, B. 1986, ApJ, 304, 1
Penny, M. T., Henderson, C. B., & Clanton, C. 2016, ApJ, submitted (arXiv:1601.02807)
Poindexter, S., Afonso, C., Bennett, D. P., et al. 2005, ApJ, 633, 914
Refsdal, S. 1966, MNRAS, 134, 315
Smith, M. C., Mao, S., & Paczyński, B. 2003, MNRAS, 339, 925
Spergel, D., Gehrels, N., Baltay, C., et al. 2015, arXiv:1503.03757
Street, R. A., Udalski, A., Calchi Novati, S., et al. 2016, ApJ, 819, 93
Udalski, A., Yee, J. C., Gould, A., et al. 2015, ApJ, 799, 237
Werner, M. W., Roellig, T. L., Low, F. J., et al. 2004, ApJS, 154, 1
Yee, J. C. 2013, ApJL, 770, L31
Yee, J. C., Gould, A., Beichman, C., et al. 2015a, ApJ, 810, 155
Yee, J. C., Udalski, A., Calchi Novati, S., et al. 2015b, ApJ, 802, 76
Zhu, W., Calchi Novati, S., Gould, A., et al. 2015, ApJ, submitted (arXiv:1510.02097)